Aeroelastic Design of Blended Composite Structures using Lamination Parameters

Terence Macquart*, Noud Werter†, and Roeland De Breuker‡

The design of composite structures based on fibre angle optimisation rapidly becomes intractable as the number of design variables increases. Lamination parameters can be used instead as intermediate design variables in order to overcome this issue. An extra step is then required in order to convert the optimal design expressed in lamination parameter into feasible blended stacking sequences. However, disparities between the lamination parameter and stacking sequence designs performance are generally observed due to discrepancies between both design spaces. In this paper, the lamination parameter blending constraints recently proposed by the authors are applied to the aeroelastic optimisation of the common research wing model in order to diminish these discrepancies and achieve more realistic lamination parameter designs. A comparison between the optimised designs achieved with and without the proposed blending constraints is carried out to evaluate our approach. Results demonstrate that the application of blending constraints greatly increases the matching quality between lamination parameter and stacking sequence designs, consequently facilitating the retrieval of equivalent blended stacking sequences.

I. Introduction

Over the last decade numerous investigations highlighting the weight saving potential of composite material have resulted in a steady incremental use of composites in primary aerospace structures. Optimising ready-to-manufacture composite structures, nonetheless, raises several challenges including the large number of design variables, manufacturing constraints and the mixed-integer‘ design space. Typical manufacturing constraints to consider are divided into laminate design, ply drop, and global structure continuity constraints.[1] Although it can be argued that the enforcement of these constraints during the optimisation process can have a significant impact on the manufacturability of the achieved design, their implementation

*Researcher, ACCIS - Advanced Composites Centre for Innovation and Science, University of Bristol, BS8 1TR, UK
†PhD Student, Department of Aerospace Structure and Material, Kluyverweg 1 2629 HS Delft, AIAA Member
‡Assistant professor, Department of Aerospace Structure and Material, Kluyverweg 1 2629 HS Delft, AIAA Member

during optimisation remains challenging.[2]

Composite optimisation algorithms can be broadly divided into two groups, namely multi-step (i) direct and (ii) indirect optimisations. Single step optimisations, omitted here, can also be found in the literature but are generally not manageable for large scale problems.[1,2] That is, single step optimisation are holistic and must encompass the whole problem complexity and optimise all design variables at once. As a result, this often leads to large number of design variables, both continuous and discrete requiring the use a meta-heuristic algorithms subject to the curse of dimensionality. It should, nonetheless, be noted that Bruyneel et al.[3] have proposed reformulating the discrete optimisation problem into an equivalent continuous one employing a shape functions with penalization approach. While promising, their approach remains limited to pre-defined fibre angles and fixed thickness. For most cases, the application of single step composite optimisations employing meta-heuristic algorithms becomes rapidly cumbersome and time consuming as the number of design variable increases. That explains, in part, the increasing number of investigation based on multi-step algorithm for composite optimisations.

In the multi-step direct optimisation framework, fibre angles and ply thicknesses are used as design variables. In order to overcome the large number of design variables, direct optimisations often involve multiple steps during which the number of composite patches is progressively refined. Within this framework Zhou et al.[4] proposed a three-step method including the super-ply, ply-bundle and ply-shuffling steps. Super-plies are first used for free size optimisation. Each fibre angle has a corresponding super-ply spanning the entire discretised structure. The thicknesses of the discretised elements are then used as design variables and optimised in order to identify dominant structural trends. The design is then progressively refined with ply-bundles and plies that can each be optimised. Ghiasi et al.[5] proposed a layerwise optimisation method, namely the layer separation approach. This approach sequentially optimises composite laminates based on a small number of layer design variables at each step. Starting from an initial laminate, the dominant layer within the laminate is identified and split into two layers. These are optimised and the process is then repeated until convergence. More recently, Jutte et al.[6] carried out an aeroelastic tailoring study of the common research model using a discrete refinement approaches combined with a genetic algorithm (GA). Although employing the direct optimisation framework is often challenging due to high-dimensionality and mixed design variables, working with fibre angles and ply thicknesses allows a direct integration of manufacturing constraints during the optimisation.

In comparison with direct approaches, stacking sequences are parametrised and intermediate continu-

ous design variables are used in the indirect framework. The initial problem can therefore be reformulated into a continuous optimisation for which fast converging gradient based algorithms are available. While designs achieved at this intermediary stage generally highlight the significant tailoring capabilities of composite materials, these designs may not be representative of realistic manufacturable composite structures. Evaluating the performance of composite tailoring based on these intermediate designs is therefore debatable since the existence of equivalent feasible stacking sequences is not guaranteed. Consequently, a second discrete optimisation step is always required in order to retrieve stacking sequences from the intermediate designs. Along this line of work, Herencia et al.[7] have used a two-level approach in which a gradient-based optimiser is employed to optimise lamination parameters while equivalent stacking sequences are retrieved with a GA. Herencia et al. do not, however, observe significant discrepancies between both level designs because their structural example is divided into substructures such as skins and stiffeners. Corresponding stacking sequences for each substructure are then retrieved individually, therefore avoiding the typical blending problem associated with multi-patch composites and ply drops. Similar approaches by IJsselmuiden et al.[8] and Liu et al.[9] employed a bi-step continuous-discrete optimisation in which a patch-based lamination parameter approach is applied to the 18-panel horseshoe problem. Montemurro et al.[10] and Catapano et al.[11] have proposed a discrete two-level optimisation strategy employing an in-house GA. In this approach, each structural part is first optimised as a single equivalent homogeneous layer employing polar formalism before matching stacking sequences are retrieved in a second optimisation step. Recently, Liu et al.[12] proposed an improvement upon their previous bi-level optimisation strategy. In particular, they proposed to employ a modified objective function during the stacking sequence retrieval from lamination parameters in order to improve the quality of retrieved stacking sequences. The modified objective includes three quantities representing the quality of the lamination parameter match, a measure of stacking sequence homogeneity and a ply angle jump index. Bohrer et al.[13] and Dutra et al.[14] both proposed an iterative approach based on the use of pre-computed stacking sequence database. A gradient-based optimiser in lamination parameter space is employed to compute the first step change in the continuous design before an equivalent stacking sequence is retrieved. The retrieved design is then used as the new starting point for the gradient-based optimiser and the process is repeated until convergence. The advantage of this strategy resides in the pre-computed stacking sequence database which spans the lamination parameter design space and permit to retrieve equivalent stacking sequence designs at each gradient step. Although numerous works on multi-step optimisation employing tow-steered composites have recently been published[15,16], the present paper focuses on patch-based composite designs for which the authors have previously derived blending constraints.

In view of its capability to handle large scale composite optimisation problems, the present study fo-

cuses on the indirect framework employing a continuous parametrisation based on lamination parameters. As noted by numerous researchers , retrieving ready-to-manufacture yet robust stacking sequences closely matching the intermediate lamination parameter design often turns out to be challenging due to manufacturing constraints.[8,9,17,18] Because of the mismatch between the two optimisation steps the retrieved stacking sequence designs are likely to have unpredicted performance requiring an iterative design procedure.[19] In particular, ensuring blending of the retrieved stacking sequences is essential to ensure a minimum level of structural continuity. Until recently, however, no blending constraints formulation for optimisation in lamination parameter spaces were available and most methods proposed in the literature have been enforcing blending during the stacking sequence retrieval step employing evolutionary algorithms.[20,21] By contrast, the aim of the present paper is to investigate the application of blending constraints in lamination parameter space as a means of achieving more realistic continuous designs, consequently facilitating the retrieval of equivalent blended stacking sequences. For that purpose, the lamination parameter blending constraints recently proposed by the authors are applied to the aeroelastic design of the common research wing model (CRM)[22] in order to reduce discrepancies between the intermediate lamination parameter design and the final stacking sequences.

The rest of this paper is structured as follows. Lamination parameters are concisely introduced in Section II. A brief introduction to blending constraints in lamination parameter space is given in Section III. The multi-step continuous/discrete optimisation used in this study is detailed in Section IV. The last Sections V-VI, conclude and evaluate the benefits of applying continuous blending constraints during the aero-structural optimisation of the CRM aircraft wing.

II. Lamination Parameters

Lamination parameters, initially proposed by Tsai and Hahn,[23] provide a convenient and compact continuous parametrisation for composite laminates. Twelve lamination parameters and one thickness variable are sufficient to fully describe any laminate layup. The lamination parameters can further be divided into three types corresponding to the in-plane, out-of-plane and coupled structural responses of the laminate. The lamination parameters notation used in this study is defined as in Eq. 1.

$$\boldsymbol{LP} = [V_1^A\, V_2^A\, V_3^A\, V_4^A\, ,\, V_1^B\, V_2^B\, V_3^B\, V_4^B\, ,\, V_1^D\, V_2^D\, V_3^D\, V_4^D]^T \tag{1}$$

where, the lamination parameters related to the laminate in-plane, out-of-plane and coupled responses are respectively denoted by V_k^A,V_k^D and V_k^B with $k = 1, 2, 3, 4$. These can be calculated for a N-ply laminate as shown in Table 1.

Table 1 Lamination parameters. Numerical evaluation for constant ply thickness.

In-plane	Coupled	Out-of-Plane
$V_1^A = \frac{1}{N}\sum_{i=1}^{N}\cos(2\theta_i)$	$V_1^B = \frac{2}{N^2}\sum_{i=1}^{N}(Z_i^2 - Z_{i-1}^2)\cos(2\theta_i)$	$V_1^D = \frac{4}{N^3}\sum_{i=1}^{N}(Z_i^3 - Z_{i-1}^3)\cos(2\theta_i)$
$V_2^A = \frac{1}{N}\sum_{i=1}^{N}\sin(2\theta_i)$	$V_2^B = \frac{2}{N^2}\sum_{i=1}^{N}(Z_i^2 - Z_{i-1}^2)\sin(2\theta_i)$	$V_2^D = \frac{4}{N^3}\sum_{i=1}^{N}(Z_i^3 - Z_{i-1}^3)\sin(2\theta_i)$
$V_3^A = \frac{1}{N}\sum_{i=1}^{N}\cos(4\theta_i)$	$V_3^B = \frac{2}{N^2}\sum_{i=1}^{N}(Z_i^2 - Z_{i-1}^2)\cos(4\theta_i)$	$V_3^D = \frac{4}{N^3}\sum_{i=1}^{N}(Z_i^3 - Z_{i-1}^3)\cos(4\theta_i)$
$V_4^A = \frac{1}{N}\sum_{i=1}^{N}\sin(4\theta_i)$	$V_4^B = \frac{2}{N^2}\sum_{i=1}^{N}(Z_i^2 - Z_{i-1}^2)\sin(4\theta_i)$	$V_4^D = \frac{4}{N^3}\sum_{i=1}^{N}(Z_i^3 - Z_{i-1}^3)\sin(4\theta_i)$

with $Z_i = -N/2 + i$ and θ_i is the fibre angle of ply i. Linear combinations of lamination parameters can then be used to retrieved the equivalent in-plane, out-of-plane and coupled stiffness matrices usually denoted as $[A]$,$[D]$ and $[B]$. For sake of brevity, readers are invited to the following references[18,24,25] for more details. Note that in this paper only in-plane lamination parameters are used. The coupled lamination parameters are zero since only symmetric laminates are investigated.

III. Blending Constraints

A recently published paper by the authors summarises the derivation of blending constraints in lamination parameter space.[26] A brief explanation about blending constraints is provided in this section due to its relevance with the present research paper. The key idea behind the derivation of blending constraints for multi-patch laminates is to quantify the change in lamination parameter due to ply-drops. Let us start by calculating the first in-plane lamination parameter for a N-ply laminate as in Eq. 2 and its corresponding value after 'X' plies have been dropped as in Eq. 3.

$$V_1^A{}_{(N)} = \frac{1}{N}\sum_{i=1}^{N}\cos(2\theta_i) \tag{2}$$

$$V_1^A{}_{(N-X)} = \frac{1}{N-X}\sum_{j=1}^{N}\cos(2\theta_j), \text{ with } j \neq \{S\} \tag{3}$$

where, $\{S\}$ denotes the set of removed plies. Note that, as in Eq. 2, the derivation of blending constraints implicitly assumes that all plies in the laminate have the same thickness. Now consider the change in the lamination parameter V_1^A due to a ply-drop as illustrated in Figure 1. The change in lamination parameter from the N-ply laminate caused by a drop of X plies can be calculated by subtracting Eq. 3 from Eq. 2 as

shown in Eq. 4.

$$\begin{aligned}\Delta V_1^A{}_{(N)\to(N-X)} &= V_1^A{}_{(N)} - V_1^A{}_{(N-X)} \\ &= \underbrace{\frac{1}{N}\sum_{k=1}^{N}\cos(2\theta_k)}_{\text{Dropped Plies}} + \underbrace{\left(\frac{1}{N}-\frac{1}{N-X}\right)\sum_{j=1}^{N}\cos(2\theta_j)}_{\text{Plies present in both laminates}}, \quad \text{with} \quad k \in S, j \notin S\end{aligned} \tag{4}$$

The left hand side of Eq. 4 is understood as the change in the first in-plane lamination parameter from a N-ply laminate to a 'N-X' ply laminate occurring due to 'X' ply drops. In order to find the maximal change in the first in-plane lamination parameters due to ply-drops we maximise Eq. 4 with respect to the ply angles. The change in lamination parameter is found to reach a maximal value of:

$$\max_{\theta_i,\theta_j}|\Delta V_1^A{}_{(N)\to(N-X)}| = 2\frac{X}{N} \tag{5}$$

For a 2-ply laminate the maximal and minimal change of the first in-plane lamination parameter respectively occur for $[0°/90°]$ and for $[90°/0°]$ at which the magnitude of $|\Delta V_1^A{}_{(N)\to(N-X)}| = \frac{2}{N}$. This results is somewhat intuitive since the greatest disparity between the in-plane stiffness of a single ply occurs for the 0° and 90° angles. Dropping the 90° ply from a $[0°/90°]$ laminate will therefore results in the maximal stiffness change that can occur due to a ply-drop for a 2-ply laminate. This explanation can readily be extended to any number of plies. That is, the maximal change of the first in-plane lamination parameter for a N-ply laminate subject ot 'X' drops will occur when 'N-X' ply angles are 0° and the 'X' dropped plies are 90°. Additionally, Eq. 5 include the ratio of the ply drops over the number of plies which simply indicates that as the number of plies increases the impact of a single ply drop on the overall structural response decreases as one would expect.

According to the above, the change of the first in-plane lamination parameter between patches can be

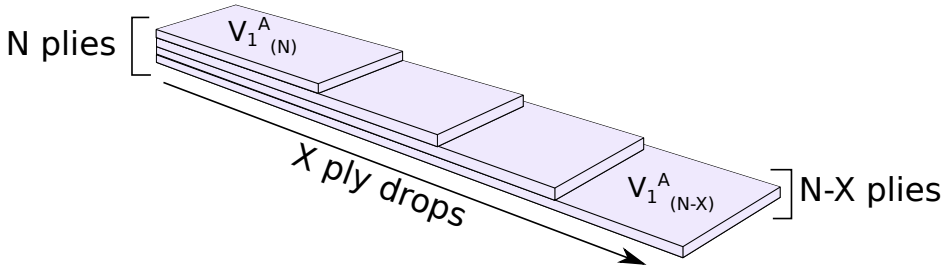

Fig. 1 Multi-patch laminate and ply-drops illustration

constrained as follows:

$$|\Delta V_1^A{}_{(N)\rightarrow(N-X)}| \quad \leq \quad 2\frac{X}{N} \tag{6}$$

which implies that no blended solution can be found if the change in V_1^A between two laminates exceeds $2X/N$. Applying the same mathematical principle, it can be shown that similar constraints must hold true for the other in-plane lamination parameter as summarised by Eq. 7.

$$|\Delta V_k^A{}_{(N)\rightarrow(N-X)}| \quad \leq \quad 2\frac{X}{N}, \quad \text{for} \quad k = 1, 2, 3, 4 \tag{7}$$

Applying four individual constraints will not, however, take into account the coupling occurring between lamination parameters. In order to account for the coupling between these four blending constraints, one can combine the various change in in-plane lamination parameters to obtain the Euclidean in-plane distance (E_{IP}) as defined in Eq. 8.

$$\left(E_{IP(N)\rightarrow(N-X)}\right)^2 = \sum_{k=1}^{4} (\Delta V_k^A{}_{(N)\rightarrow(N-X)})^2 \tag{8}$$

The E_{IP} value can be understood as the norm of the vector connecting two four-dimensional points in the in-plane lamination parameter space. It can be shown that E_{IP} has to satisfy Eq. 9 for blended solutions to exist.

$$\left(E_{IP(N)\rightarrow(N-X)}\right)^2 \quad \leq \quad \beta(6.25(X/N)^2) \tag{9}$$

Simply stated, this constraint limits the lamination parameter change in a four dimensional hypersphere. The '6.25' scalar value in Eq. 9 is calculated as a combination of trigonometric functions and has been derived previously by the authors.[26] Dropping a ply from a N-ply laminate can result in the maximal distance of $6.25(1/N)^2$ between two four-dimensional lamination parameter points in the in-plane space. The added parameter β allows the radius of the sphere to be reduced since the original derived constraints (i.e. $\beta = 1$) result in excessive design freedom.[26] That is, the '6.25' value is calculated based on the maximal possible change in lamination parameter, often corresponding to very specific laminates (e.g. $[0°/90°]$). However, laminate are generally required to be somewhat homogenised as expressed by the 10% rule for composite design guidelines. As a result, the maximal change in lamination parameter directly computed with the blending constraints will never be reached in realistic laminates and the scaling coefficient β can be set to a value between zero and one to represent the allowed design freedom. Setting β to one results in a blending constraints that will never be active while setting β to zero forbids any change in lamination parameter throughout the structure. The inequality described by Eq. 9 is the main blending constraints used during

the rest of this investigation.

A two dimensional example of blending constraints in lamination parameter space is shown in Figure 2. In this example we start from a randomly generated 10-ply stacking sequence and compute its V_1^A and V_2^A lamination parameters (black dot). We then calculate the maximal Euclidean distance allowed by the blending constraints when one ply is removed (blue circle). Next, the 10 possible 9-ply stacking sequences obtainable after one ply drop are defined and their corresponding V_1^A and V_2^A lamination parameters are calculated (blue square). The process is then repeated for 3 ply drops (red circle and red cross). As can be seen in this figure, the proposed blending constraints include all possible combinations of removed plies while also significantly reducing the feasible lamination parameter space. It should be mentioned that because only two lamination parameters are considered in this example, the maximal distance is different than the one provided in Eq. 9 and is actually equal to $(4(X/N)^2)$. Note that further constraints can also be derived for out-of-plane lamination parameters and the reader is invited to the original published article for more details.[26]

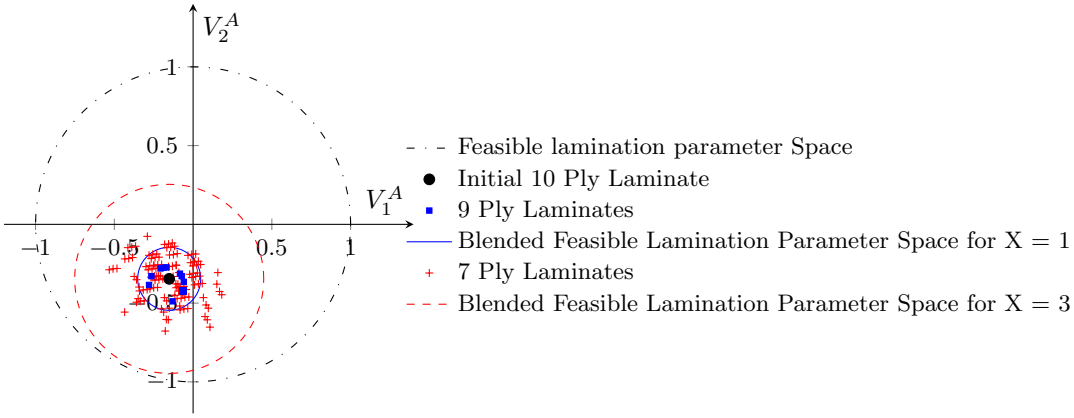

Fig. 2 A 10-ply two dimensional example of blending constraints.

IV. Optimisation Framework

In this section, the optimisation framework employed to investigate the application of blending constraints in lamination parameter space as a means of achieving more realistic continuous designs is presented. A bi-step optimisation strategy consisting of a continuous gradient based optimiser followed by a stacking sequence retrieval GA is used to design the CRM wingbox structure.

A. Continuous Optimisation

The aeroelastic performance of the CRM wing is evaluated using the in-house PROTEUS[27] framework as described in Figure 3. The purpose of the aeroelastic analysis and optimisation framework is to design and analyse conventional wingbox structures with ribs, spars, and a load bearing skin. As illustrated in Fig-

ure 4, the three-dimensional wing geometry is split into spanwise sections. Each wingbox cross-section is in turn modelled using laminates for the skins and spars. Instead of describing the composite laminates by ply angles and a stacking sequences to obtain the stiffness properties, each laminate is described by lamination parameters and the laminate thickness, resulting in a fixed number of continuous design variables per laminate.

The aeroelastic analysis and optimisation loop starts with the definition of the material properties, wing geometry and load cases as inputs. Next, using the material properties defined as input and the lamination parameters and laminate thickness generated by the optimiser, the properties of each of the laminates is computed. In order to generate the beam model, these laminate properties, together with the cross-sectional geometry, are used to generate the Timoshenko cross-sectional stiffness matrix with respect to the beam reference axis using the cross-sectional modeller developed by Ferede et al.[28] As illustrated in Figure 4, the cross-sectional modeller discretises the cross-section using linear Hermitian shell elements to obtain the Timoshenko cross-sectional stiffness matrix of any arbitrary, open or closed, thin-walled composite cross-section including spars. As a third step, a geometrically nonlinear static aeroelastic analysis is carried out to obtain the nonlinear static displacement field of the aircraft for the various load cases. The static aeroelastic analysis model monolithically couples a geometrically nonlinear Timoshenko beam model based on the co-rotational formulation to an aerodynamic model based on the vortex lattice method. Both models are closely coupled and a geometrically nonlinear aeroelastic solution is obtained by using load control and the Newton-Raphson root finding method. All analyses are performed at a trimmed flight condition, by adjusting the angle of attack such that lift equals weight, in order to compare the structural performance of the wings under equivalent aerodynamic loads. Finally, in the fourth module, the analysis results are processed and the output is generated. The module provides the deformed wing geometry and aeroelastic loads. Furthermore, from the beam deformation, the cross-sectional modeller can be used to compute the skin strains and, as such, assess the structural performance of the wing. In order to find the optimum, the globally convergent method of moving asymptotes (GCMMA) is used as a gradient-based optimiser.[29]

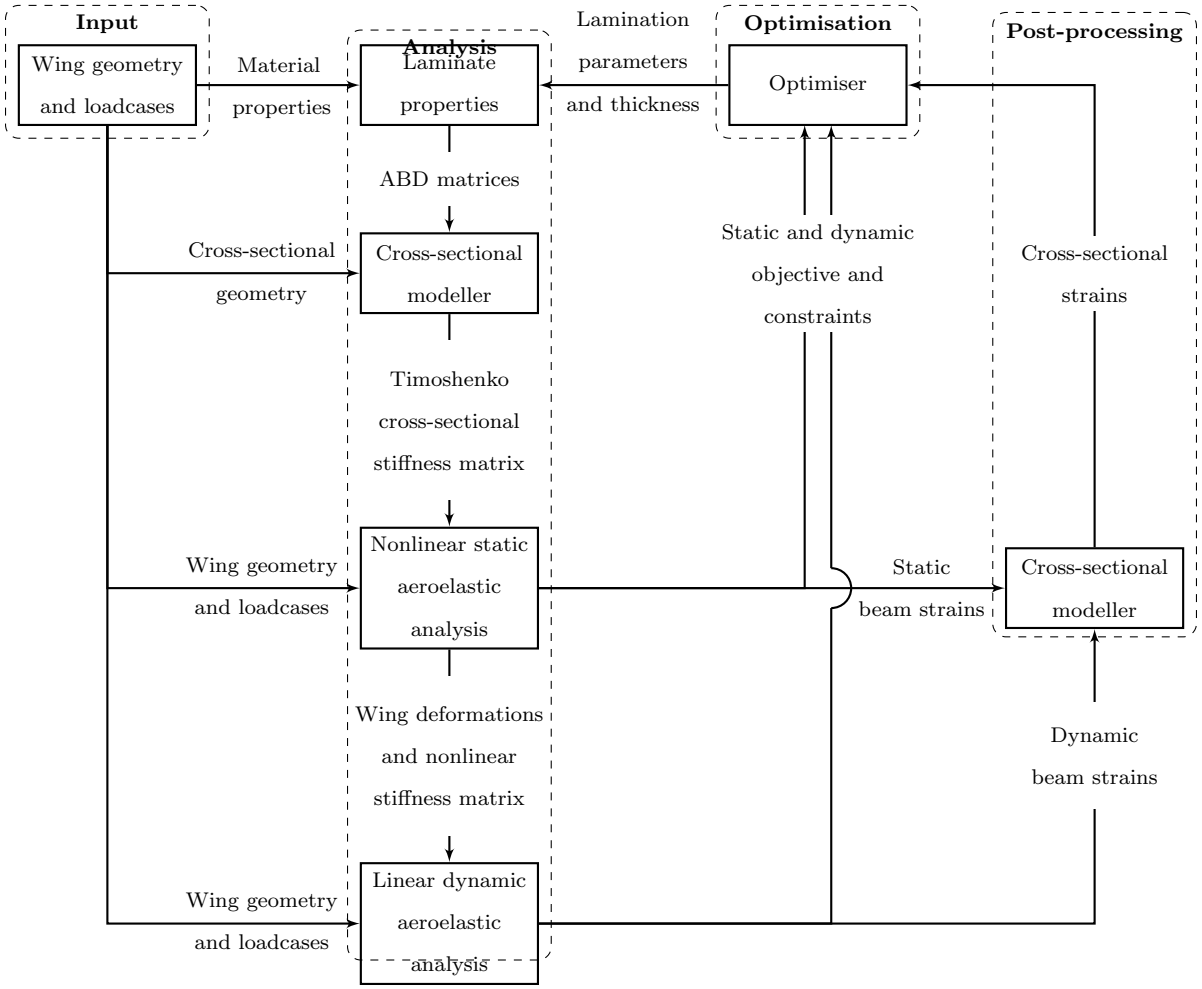

Fig. 3 PROTEUS continuous aeroelastic optimisation loop[27]

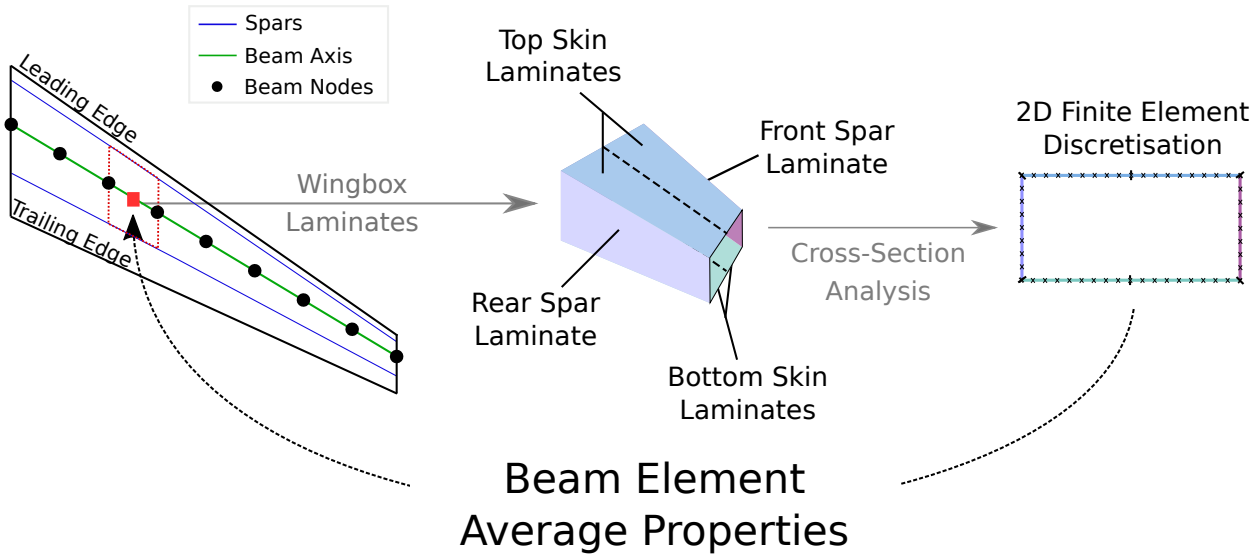

Fig. 4 Beam finite element modelling strategy

The method used to evaluate the impact of lamination parameter blending constraints onto the retrieved

stacking sequence design is illustrated in Figure 5. Two optimisation strategies, the conventional and the present strategies, are compared for this purpose. In the unblended conventional case, the lamination parameters and thicknesses are first optimised as it would normally be done without blending constraints (step 1 X_U). In step 3, a repair function rounds up the thicknesses to an even number of plies X_R for stacking sequence retrieval purpose. Note that although using an even number of plies is not necessary, the original derivation of blending constraints assumes that laminates have even number of plies in order to simplify the mathematical derivation of the constraints.[26] The repaired design (X_R) lamination parameters are optimised one last time in step 4 in order to maximise constraint satisfactions while thicknesses remain fixed. Following the fourth step, a stacking sequence retrieval GA is employed to retrieve a globally blended structure (step 5). In the blended case, step 2 is added during which the optimiser starts from the infeasible (i.e. non-blended) optimum design X_U and converges towards the closest local optima X_B satisfying all constraints including blending. The blended optimisation includes an extra step because enforcing the blending inequality (Eq. 9) constraints while optimising for both thicknesses and lamination parameters results in a non-convex optimisation.[26]

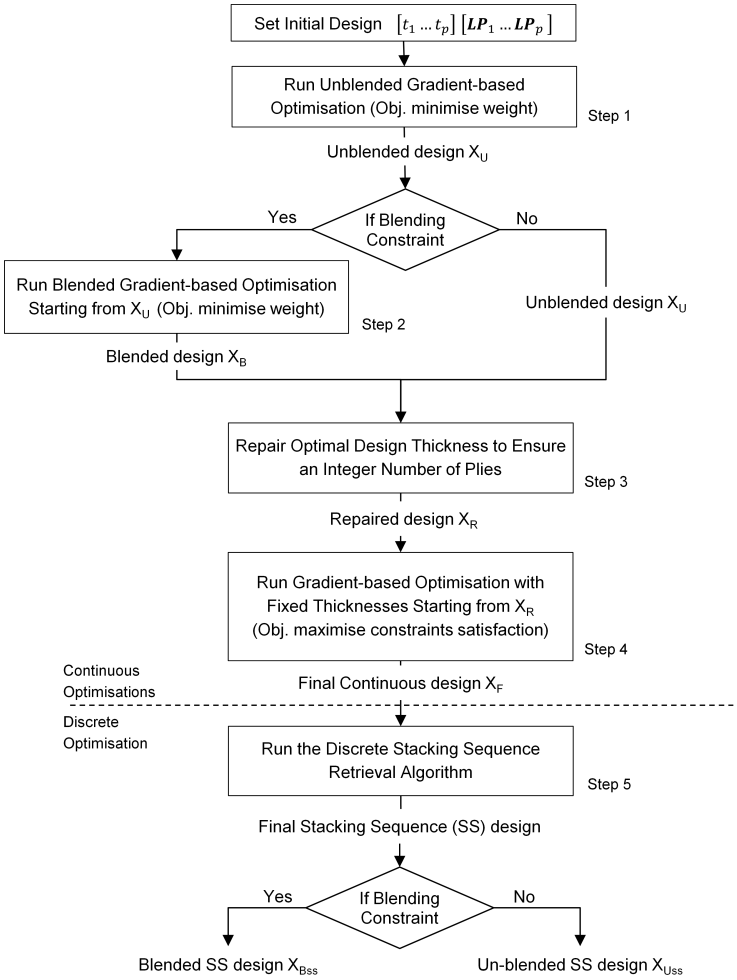

Fig. 5 Algorithm employed for composite optimisation including blending constraints in lamination parameter space

B. Stacking Sequence Retrieval

An open source stacking sequence optimisation toolbox developed by the authors is used to retrieve blended stacking sequences (https://github.com/TMacquart/OptiBLESS). Within this toolbox, a guide-based GA is employed to retrieve blended stacking sequences matching the optimised lamination parameters achieved by the continuous optimisation. According to the guide-based methodology,[21] the thickest laminate is defined as the guide-laminate. Other laminates from the same structure are obtained by dropping plies from the guide-laminate, therefore ensuring the final design is blended. Two retrieval methodologies are compared in this paper:

- The first is denoted θ_{opt} and is a fixed thickness lamination parameter matching strategy. Thicknesses obtained from the continuous optimisation remain fixed and only the fibre angles $\boldsymbol{\theta}$ and ply drops $\boldsymbol{\Xi}$ of the guide laminates are used as design variables.

- The second is referred to as $\theta_{opt} + N_{opt}$ and is a variable thickness lamination parameter matching strategy. In this case, thicknesses obtained from the continuous optimisation are used as a baseline around which the number of plies is allowed to vary in addition to fibre angles and ply drops.

The genotypes used by the GA in order to describe each blended solution depending on the methodology used can be represented as shown in Table 2.

Table 2 Genotype coding for blended stacking sequences

Optimisation Strategy	Number of Plies	Guide Fibre Angles	Ply Drops
θ_{opt}	N/A	$\theta_1\ \theta_2\ ...\ \theta_m$	$\Xi_1\ \Xi_2\ ...\ \Xi_q$
$\theta_{opt} + N_{opt}$	$N_1\ N_2\ ...\ N_p$	$\theta_1\ \theta_2\ ...\ \theta_m$	$\Xi_1\ \Xi_2\ ...\ \Xi_q$

Once individuals are fed to the fitness evaluation function of the GA, they are decoded and their corresponding lamination parameters are calculated and used to evaluate their fitnesses. Since it is expected that the final continuous design at the end of step 4 will be more realistic due to the application of blending constraints, it is likely that a close equivalent of this design can be found in the fibre angle space. In order to take advantage of this design equivalence and to avoid the computation of a potentially expensive aeroelastic fitness function, the objective of the guide-based GA is to match the lamination parameters of the optimal continuous design. Accordingly, a fitness function based on the root mean square error (RMSE) between the continuously optimised lamination parameters and the retrieved one is used to evaluate the quality of individuals as defined in Eqs.10 and 11.

$$\min(Fitness(\boldsymbol{\theta}, \boldsymbol{\Xi}, \boldsymbol{N})) = \min\left(\frac{1}{N_{lam}} \sum_{p=1}^{N_{lam}} RMSE_p(\boldsymbol{\theta}, \boldsymbol{\Xi}, \boldsymbol{N})\right) \tag{10}$$

$$RMSE_p(\boldsymbol{\theta}, \boldsymbol{\Xi}, \boldsymbol{N}) = \sqrt{\frac{1}{12} \sum_{i=1}^{12} \left(\widetilde{\boldsymbol{LP}}_{i,\,p} - \boldsymbol{LP}_{i,\,p}(\boldsymbol{\theta}, \boldsymbol{\Xi}, \boldsymbol{N})\right)^2} \tag{11}$$

where, $\widetilde{\boldsymbol{LP}}_{i,\,p}$ is the vector of input lamination parameters for laminate p and $\boldsymbol{LP}_{i,\,p}$ is the vector of lamination parameters obtained by the GA. In the following section example only symmetric plies are used and the coupled laminations parameters V_i^B are zero Note that all lamination parameters are weighted equivalently. However, from a physical point of view, some lamination parameters at critical parts of the wing have more influence on the design performance and should ideally be prioritised when retrieving a matching stacking sequence as noted by previous research.[8] While the inclusion of weights for each lamination parameter is likely to permit a more robust stacking sequence retrieval, the definition and comparison of different weight is outside the scope of the present paper.

V. Evaluating the Impact of Blending Constraints

A. A Benchmarck Model

The NASA common research model originally developed for the 4th AIAA drag prediction workshop[22] is used as a case study during this investigation. The CRM is one of the few available models representative of a wide body transonic commercial transport aircraft. The aircraft wing's main characteristics and operating condition are summarised in Table 3 and Figure 6. A more detail illustration of the wing planform, wingbox and the discretised finite element model are depicted in Figure 7. The wingbox geometry has been derived from the finite element model made publicly available by NASA. The wingbox is composed of two spars and the top and bottom skins are divided into 20 laminates each. Note that while the entire wingbox is made of composite materials, results will often be presented for the top skin only for sake of brevity. A quasi-isotropic initial design with maximal thickness near the engine location is used as initial starting point of the continuous optimisation. The corresponding patch normalised polar stiffnesses are plotted on the wing planform, this is represented by the black circle (i.e. quasi-isotropic) in Figure 8. Note that, buckling is not considered during this investigation and out-of-plane lamination parameters are not used since the wing bending behaviour is mostly dominated by in-plane stiffness.

Table 3 CRM wing main features

Span (m)	58.7629
Quater chord Edge Sweep Angle ($^\circ$)	35
Wimpress - Wing Aspect Ratio	9
Taper Ratio (λ)	0.275
Wimpress Wing Area (m^2)	383.67
Cruise Mach number	0.85

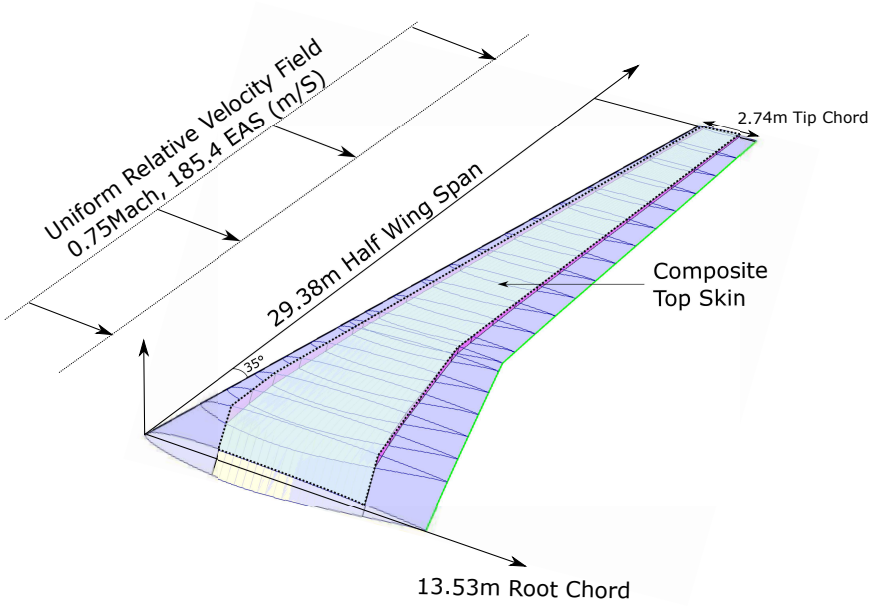

Fig. 6 CRM wing model operating condition used in this study

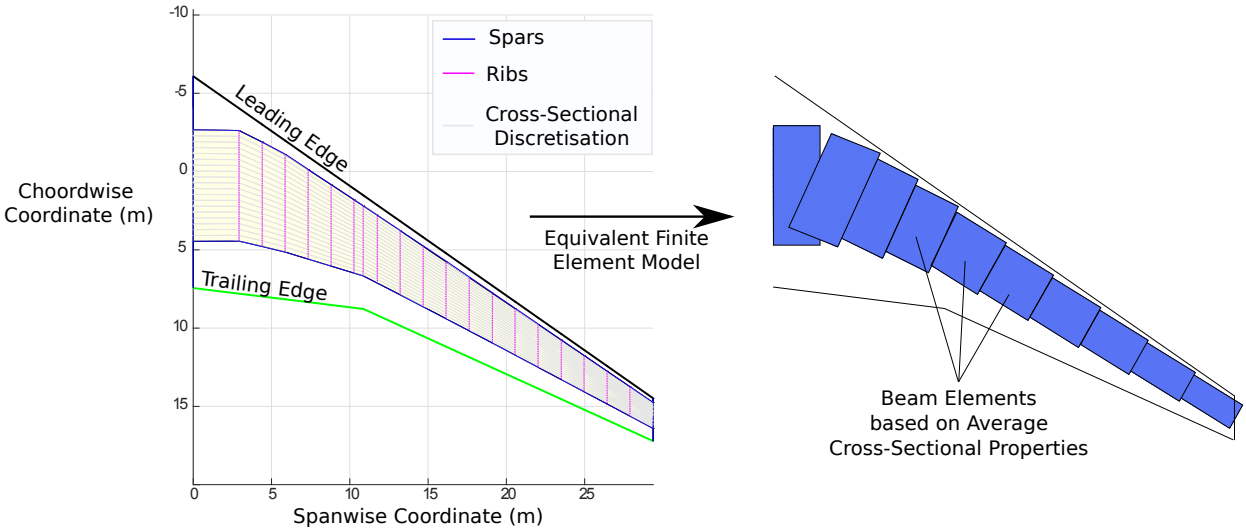

Fig. 7 CRM structural wing model and finite element representation

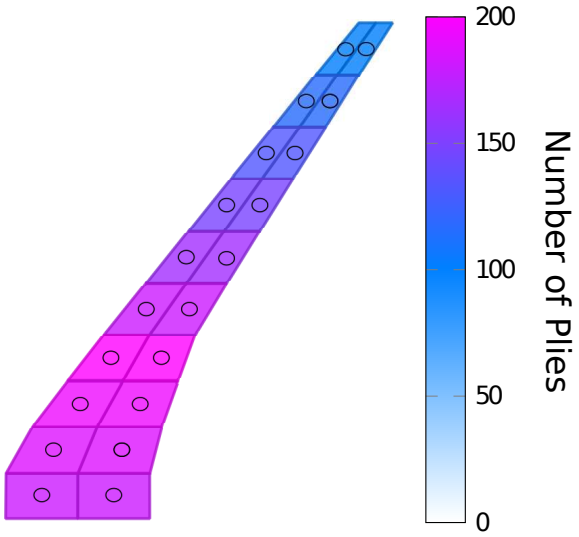

Fig. 8 CRM wing top skin initial thickness and stiffness distribution

B. Continuous Aeroelastic Optimisation

The continuous optimisation results obtained with and without the application of blending constraints (i.e. X_U and X_B) are presented in this section. As illustrated in Figure 6, a typical +2.5g load case occurring at a Mach number 0.75 is used during this investigation. The optimisation problem for the first and second steps is formulated as follows:

$$\min(weight) = \min f(N_p) = \min \sum_{p=1}^{N_{lam}} A_p \rho_p N_p t_{ply}$$

$$s.t.$$

$$|\epsilon_p(t_p, \boldsymbol{LP}_p)| \leq 0.0045$$

$$|\gamma_p(t_p, \boldsymbol{LP}_p)| \leq 0.0070$$

$$|\alpha| \leq 15\,\text{deg}$$

$$\left(E_{IP_{(p_1)\rightarrow(p_2)}}\right)^2 \leq \beta(6.25(X/N)^2), \quad (step2)$$

where, A_p, ρ_p, t_{ply} and $\boldsymbol{LP}_p$ respectively denote the p_{th} laminate area, density, ply thickness and lamination parameters. The constraints ϵ, γ, and α refer to axial and shear strain limits including knockdown factors for environmental effects and material scatter,[30] and trim condition (i.e. maximum local angle of attack allowed). The blending constraint is checked for each couple of laminate patches in the structure as expressed by $(p_1) \rightarrow (p_2)$ and the scaling parameter is set to $\beta = 0.5$. As previously explained in Section IV, the blending constraints are not used during the first optimisation step.

After step three during which the number of plies are round off, the thickness are fixed and the optimisa-

tion problem is re-formulated in step four in order maximise constraint margins. The minimisation function employed in step four can be written as follows:

$$\min \sum_{k=1}^{m} g_k$$

$$s.t.$$

$$|\epsilon_p(t_p, \boldsymbol{LP}_p)| \leq 0.0045$$

$$|\gamma_p(t_p, \boldsymbol{LP}_p)| \leq 0.0070$$

$$|\alpha| \leq 15\,\mathrm{deg}$$

$$\left(E_{IP\,(p_1)\rightarrow(p_2)}\right)^2 \leq \beta(6.25(X/N)^2)$$

where, the g_k's represent the constraints written as equality constraints (e.g. $|\epsilon_1(t_1, \boldsymbol{LP}_1))|-0.0045 = g_1$). In addition to enforcing that the g_k's must be negative in order for the constraints to be satisfied, we maximise the constraints margin by minimising the g_k's values.

Results for the wing top and bottom skins are respectively shown in Figures 9 and 10. In these figures, the thickness distribution obtained after continuous optimisation without the application of blending constraints is referred to as *unblended* X_U. The increase in thickness occurring due to the application of the blending constraints is shown next to it (X_B). Finally the difference in stiffness between both optimal designs is presented on the figures' right hand side. The main discrepancy between both designs is identified as the significant increase in thickness. By contrast, it can be seen that the stiffness distribution between both designs are nearly identical. Since stiffnesses remain almost unchanged, thickness increase is the primary method used by the optimiser to satisfy blending constraints. This occurs because the blending inequality constraint gradient is dominated by the thickness derivatives (see Eq. 9).

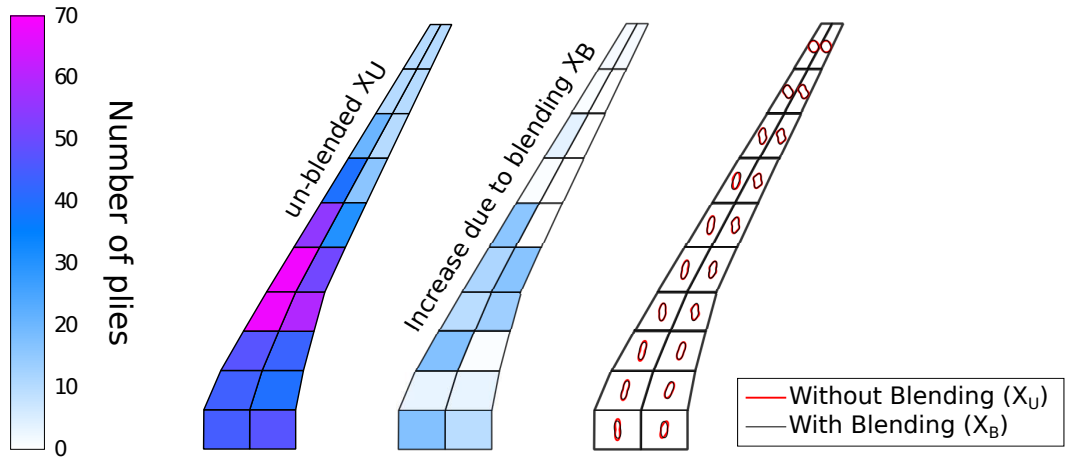

Fig. 9 Optimised top skin thickness and stiffness with and without blending constraints

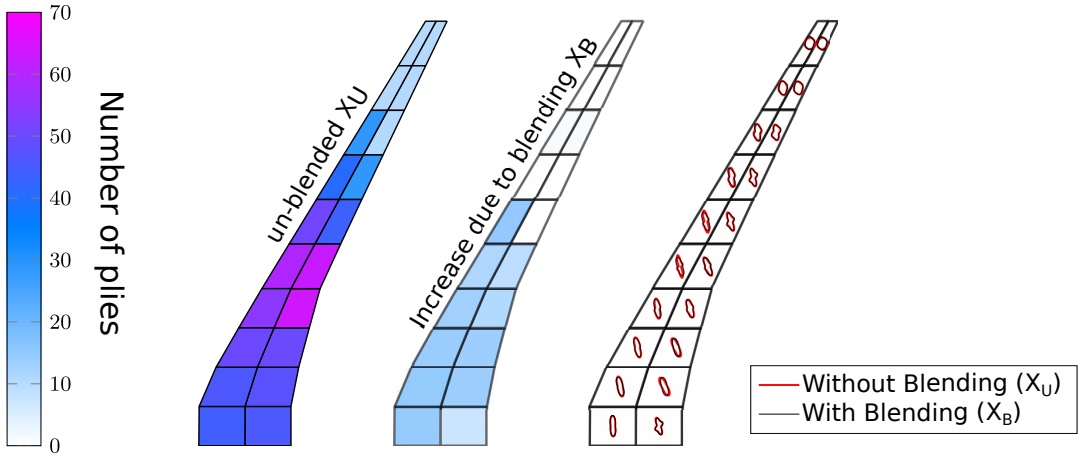

Fig. 10 Optimised bottom skin thickness and stiffness with and without blending constraints

The top skin strain distribution results obtained for both continuous designs are compared in Figure 11. Results for the axial and shear strains achieved without blending constraints X_U are presented on the left side of the figure. The optimiser reaches the feasible design space boundary as can be seen by the limit strain values of -4500 and 7000 distributed along the wing span. The strain distributions obtained due to the application of the blending constraints X_B are shown in the right side of this figure. As expected, a reduction of the axial and shear strain is observed towards the root and the engine location where thickness has increased. Although some small variations can also be observed, it is reasonable to affirm that overall both designs are driven by the same strain constraints.

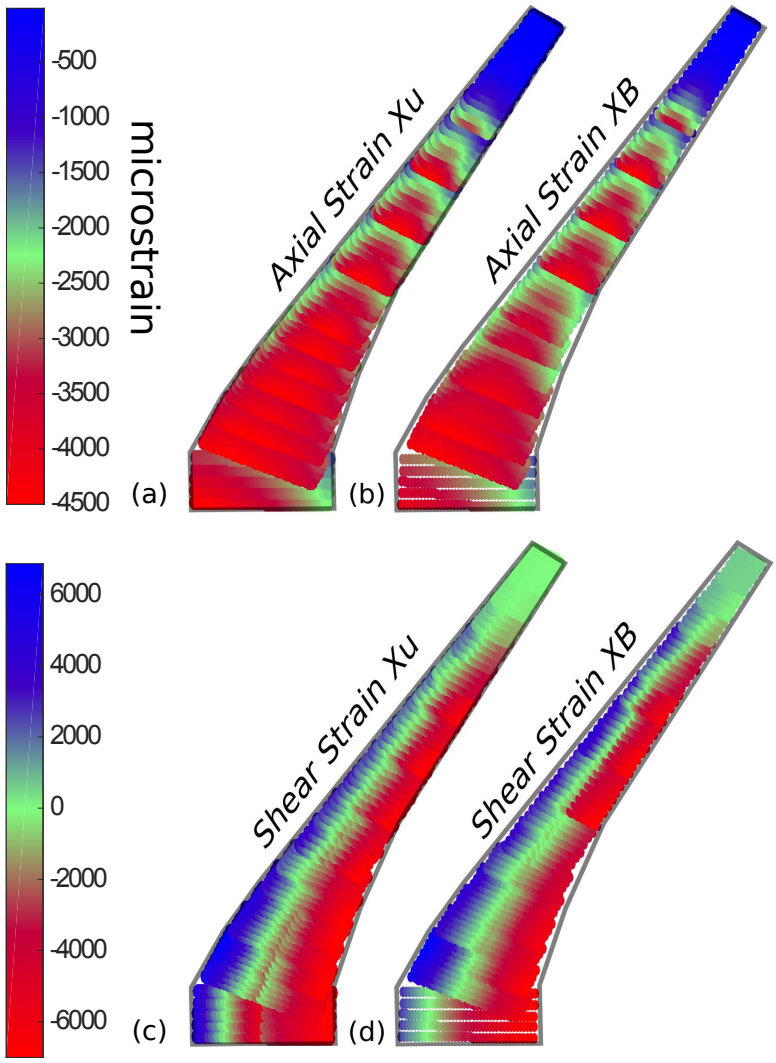

Fig. 11 Top skin axial (a,b) and shear (c,d) strains for the unblended and blended designs

C. Retrieved Stacking Sequence Comparison

In order for the observed thickness increase due to the application of blending to be justified (see Figure 9), we evaluate the influence of blending constraints on the stacking sequence retrieval performance. The two retrieval methodologies presented in Section B are employed to retrieve stacking sequences corresponding to the two continuous designs previously obtained. Detailed stacking sequence designs are provided in appendix while general results are presented in this section.

Retrieval results presented in Figure 12 show the final number of plies and the lamination parameter matching RMS error. As expected from our previous observation, the total number of plies of the blended solution $X_{Bss}[\theta_{opt}]$ is higher than the one of the unblended $X_{Uss}[\theta_{opt}]$ design. Interestingly, the blended

solution is seen to achieve significantly better lamination parameter matching performance.The addition of blending constraints during the second optimisation step and the resulting increase in thickness near the root and engine locations were, therefore, justified in order to obtain a more realistic blended design.

Next, comparing results with the variable thickness option $X_{Uss}[\theta_{opt} + N_{opt}]$, an improvement of lamination parameter matching with respect to the fixed thickness matching $X_{Uss}[\theta_{opt}]$ is observed. However, even with variable thickness the lamination parameter RMS matching error remains high compared to the results obtained for the blended design. This suggests that the application of blending constraints has been effective in order to obtain a blended continuous design and reduce the discrepancies between the continuous and discrete steps of the optimisation.

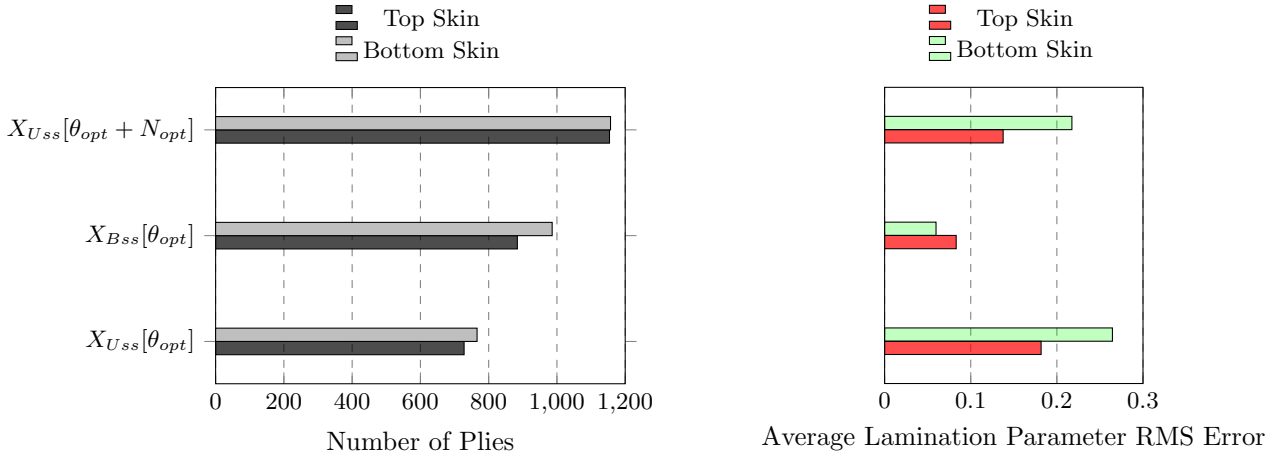

Fig. 12 Number of plies and average RMS error of retrieved stacking sequence designs

The effect of the matching discrepancies between the lamination parameter and stacking sequence designs on the aeroelastic variability of the wing performance is now investigated. Out-of-plane and in-plane deflections, and twist angles are presented in Figures 13, 14 and 15. The left hand side of these figures highlights the discrepancies between the unblended continuous design X_U and its retrieved stacking sequences. Note that while the discrepancies may be small, their impacts on the aero-structural behaviour of the wing cannot be predicted beforehand. Meaning that the performance of the retrieved stacking sequence should be re-evaluated and possibly re-optimised using the aero-structural evaluation function. By comparison, the right hand side of these figures demonstrates the nearly perfect aeroelastic match obtained between the lamination parameter and stacking sequence designs achieved whilst using blending constraints. These results imply that the application of blending constraints during the continuous optimisation in step two has successfully led to a continuous optimal design X_B that has a close equivalent in fibre angle space $X_{Bss}[\theta_{opt}]$.

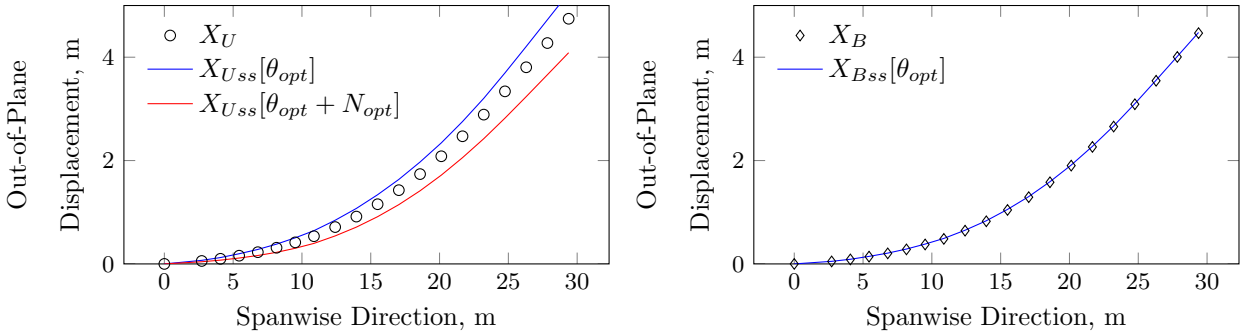

Fig. 13 Wing out-of-plane displacement
(X_U and X_B respectively denote the unblended and blended continuous design)

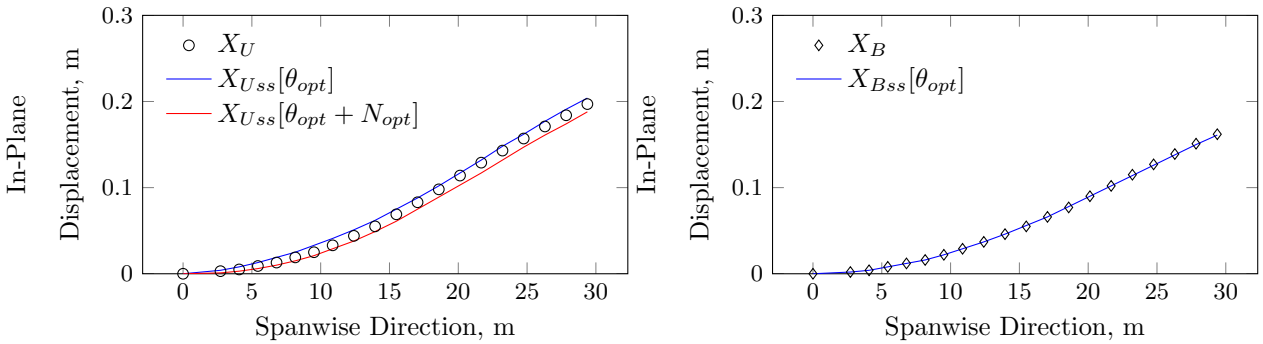

Fig. 14 Wing in-plane displacement
(X_U and X_B respectively denote the unblended and blended continuous design)

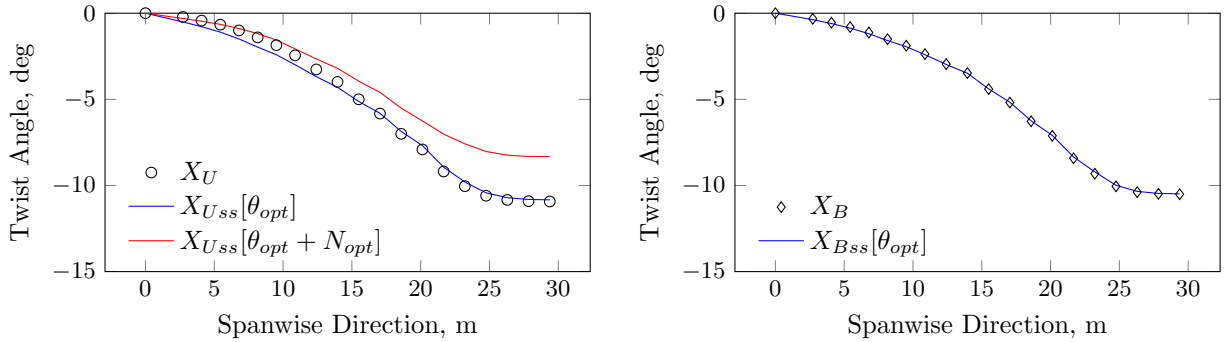

Fig. 15 Wing twist angle
(X_U and X_B respectively denote the unblended and blended continuous design)

The final results show the changes in strain distribution between the continuous and retrieved optimal designs. The left hand side of Figure 16 illustrates the variations of axial strains while the right hand side shows the variations in shear strains. As clearly illustrated by these figures, trying to retrieve stacking sequences from optimised lamination parameters obtained without blending constraints results in non-negligible change in strain distribution. By contrast, it can be seen that the application of blending constraints results in a very good strain distribution match between the lamination parameter and stacking sequence designs.

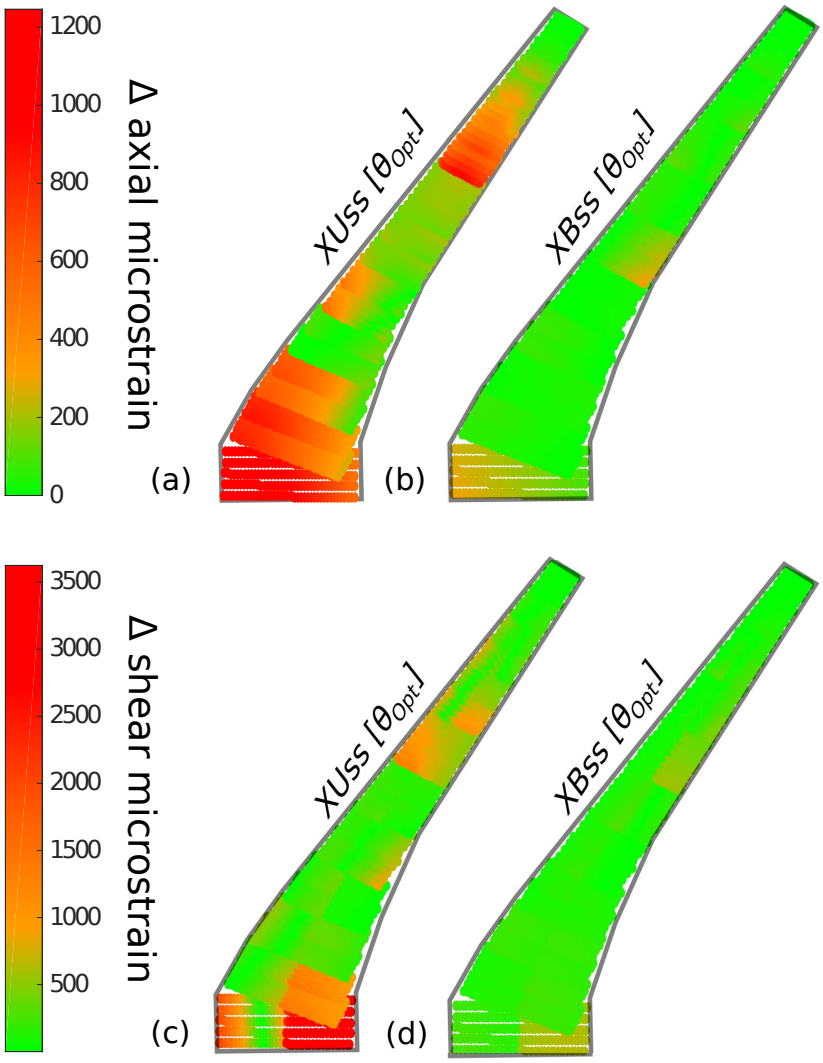

Fig. 16 Top skin absolute strain error between continuous and discrete designs

Results presented in this section highlight the difficulty encountered when using multi-step optimisation frameworks based on a continuous parametrisation. In particular, retrieving stacking sequences exactly matching results obtained at the end of the conventional continuous optimisation was shown to be challenging. The presented results suggest that the application of blending constraints in lamination parameter space successfully leads to more realistic continuous designs and that the discrepancies between the continuous and discrete designs can be successfully reduced. In other words, the application of blending constraints was shown to direct the continuous optimiser towards an optimal design with close equivalence in fibre angle space. These promising results were, however, achieved at the cost of an increase in mass with respect to the unblended continuous design. Applying blending constraints in lamination parameter space results in a trade-off between the blended-feasibility (i.e. value given to β in Eq. 9) and the mass of the optimised continuous design. In that respect, no claim is made regarding the optimality of the retrieved designed using

the proposed sequential algorithm and future work may result in further improvement.

VI. Concluding Remarks and Future Work

Exact stacking sequence retrieval for medium and large scale composite optimisation problems using an intermediate continuous parametrisation is often challenging. In most cases, stacking sequences approximating the lamination parameters will only be available due to the discrepancies between the continuous and discrete optimisation steps. As a result, unpredicted change in performance will occur between the continuous optimised design and the retrieved stacking sequences. In this paper, the authors have investigated the impact of lamination parameters blending constraints on the stacking sequence retrieval performance of an aeroelastic composite wing structure.

To summarise, it has been found that the application of blending constraints during continuous optimisation greatly increases the chances of retrieving closely matching stacking sequences. As a result, discrepancies between the continuous lamination parameter design and the discrete stacking sequence optimisation step were shown to be significantly reduced. Applying blending constraints leads to more realistic continuous design which, in turn, reduce the number of iterations required to obtain the final stacking sequences. Last but not least, the close equivalence between continuous and discrete designs permits the use of a stacking sequence retrieval algorithm based on a low computational cost fitness function such as lamination parameter matching. Overall the outcomes of this study are encouraging and blending constraints may play a key role for future patch-based composite optimisation with variable thickness.

Appendix

Example of retrieved stacking sequence from lamination parameters are presented in this section. The top skin stacking sequence retrieved from the lamination parameter design obtained without blending constraints is shown in Figure 17. By contrast, the stacking sequence design retrieved from the continuous design obtained employing the blending constraints is shown in Figure 18. As previously demonstrated, the blended solution contains more plies but also results in a better matching design as it can be observed in Table 4. Note that in this example, only the symmetric design guideline is active. The open-source optimisation toolbox[31] used for that purpose can be found at *https://github.com/TMacquart/OptiBLESS*.

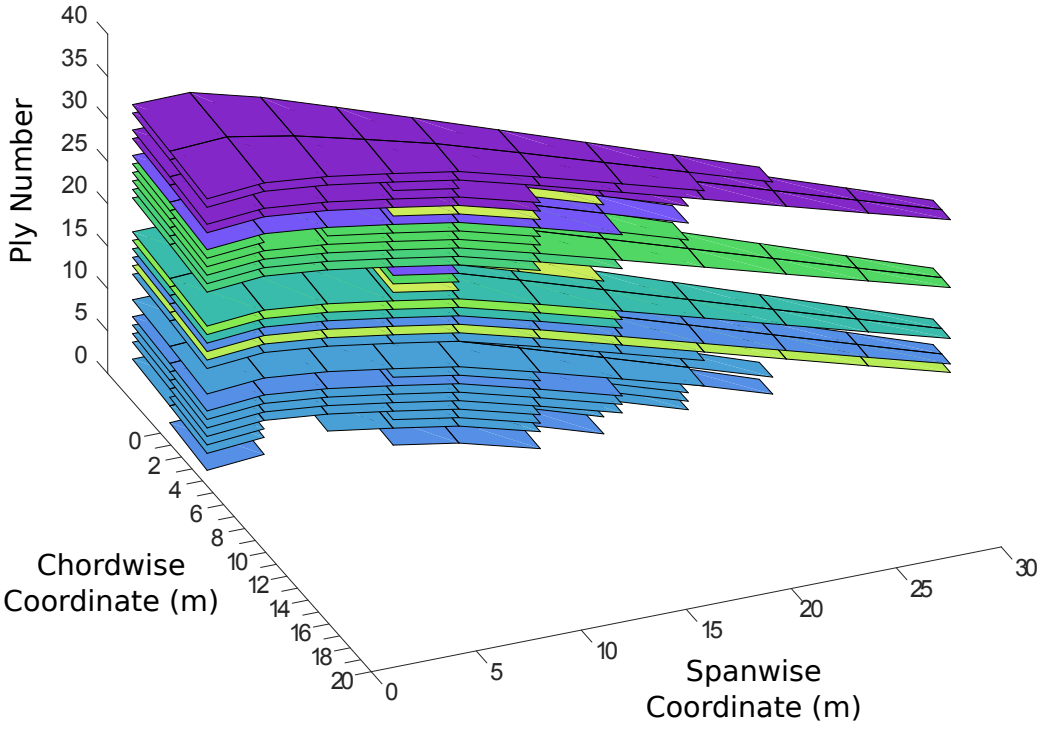

(a) Layup overview

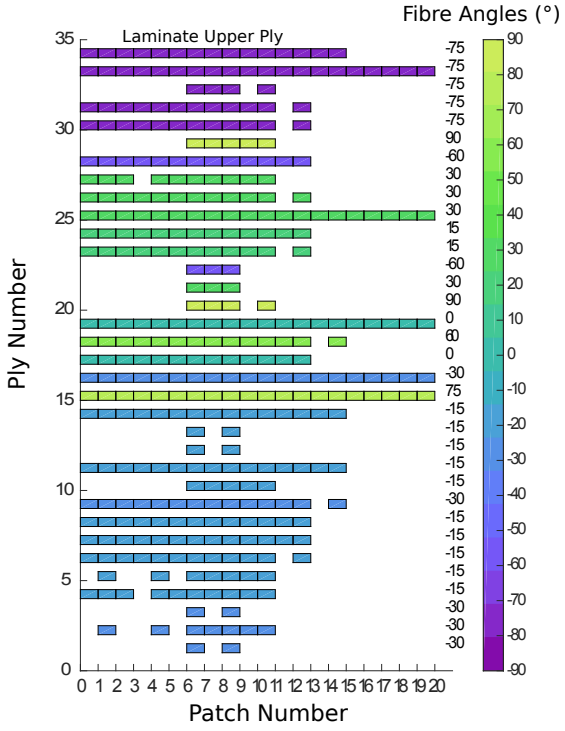

(b) Detailed layup

Fig. 17 Top skin stacking sequence optimised by OptiBLESS based on the un-blended continuous design

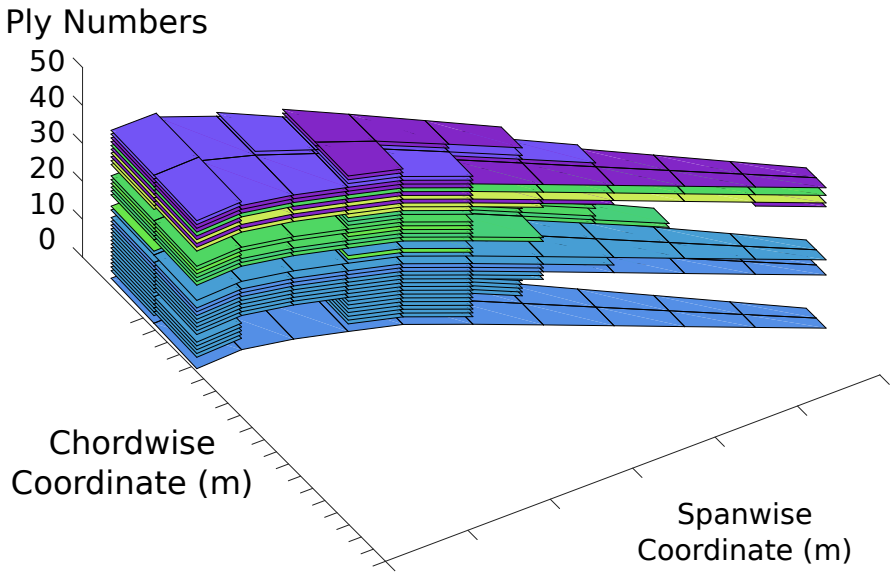

(a) Layup overview

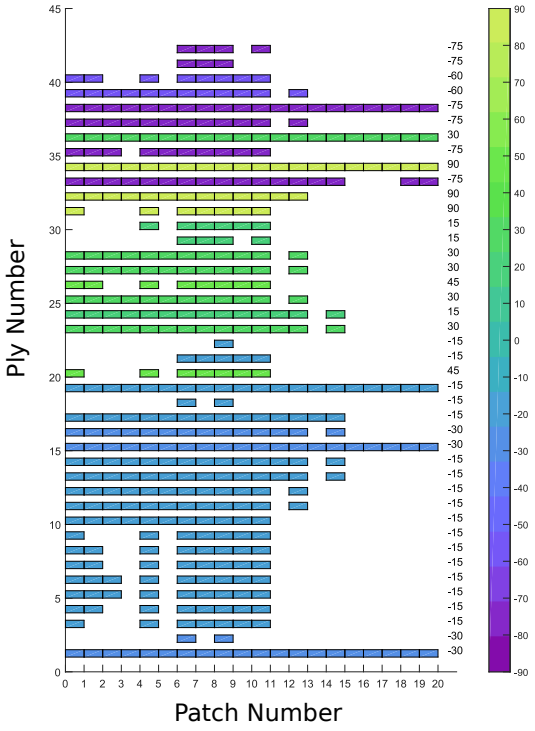

(b) Detailed layup

Fig. 18 Top skin stacking sequence optimised by OptiBLESS based on the blended continuous design

Table 4 Un-blended and blended lamination parameters matching results (average un-blended RMSE = 0.15032, average blended RMSE = 0.098738)

Patch Number	XU_{SS} RMSE	XB_{SS} RMSE	Improvement (%)
1	0.41263	0.13125	68.192
2	0.41877	0.19816	52.68
3	0.13294	0.11802	11.223
4	0.10937	0.084975	22.305
5	0.12386	0.06095	50.791
6	0.082513	0.10166	-23.205
7	0.090608	0.087154	3.812
8	0.073263	0.078507	-7.1578
9	0.11599	0.10872	6.2678
10	0.084969	0.037753	55.569
11	0.11709	0.071964	38.54
12	0.12616	0.092217	26.905
13	0.12625	0.12898	-2.1624
14	0.079744	0.096899	-21.513
15	0.12646	0.11308	10.58
16	0.14522	0.084255	41.981
17	0.16572	0.098384	40.632
18	0.17422	0.084363	51.577

References

[1]F-X Irisarri, Alexis Lasseigne, F-H Leroy, and Rodolphe Le Riche. Optimal design of laminated composite structures with ply drops using stacking sequence tables. *Composite Structures*, 107:559–569, 2014.

[2]Hossein Ghiasi, Kazem Fayazbakhsh, Damiano Pasini, and Larry Lessard. Optimum stacking sequence design of composite materials part ii: Variable stiffness design. *Composite Structures*, 93(1):1–13, 2010.

[3]Michael Bruyneel, Clément Beghin, Guillaume Craveur, Stéphane Grihon, and Masha Sosonkina. Stacking sequence optimization for constant stiffness laminates based on a continuous optimization approach. *Structural and Multidisciplinary Optimization*, 46(6):783–794, 2012.

[4]Ming Zhou, Raphael Fleury, and Martin Kemp. Optimization of composite–recent advances and application. In *13th AIAA/ISSMO Multidisciplinary Analysis Optimization Conference, Fort Worth, Texas. September*, pages 13–15, 2010.

[5]Hossein Ghiasi, Damiano Pasini, and Larry Lessard. Layer separation for optimization of composite laminates. In *ASME 2008 International Design Engineering Technical Conferences and Computers and Information in Engineering Conference*, pages 1247–1253. American Society of Mechanical Engineers, 2008.

[6]Christine V Jutte, Bret K Stanford, Carol D Wieseman, and James B Moore. Aeroelastic tailoring of the nasa common research model via novel material and structural configurations. In *AIAA SciTech Conference*, pages 13–17, 2014.

[7]J Enrique Herencia, Paul M Weaver, and Mike I Friswell. Optimization of long anisotropic laminated fiber composite panels with t-shaped stiffeners. *AIAA journal*, 45(10):2497–2509, 2007.

[8]Samuel T IJsselmuiden, Mostafa M Abdalla, Omprakash Seresta, and Zafer Gürdal. Multi-step blended stacking sequence design of panel assemblies with buckling constraints. *Composites part b: engineering*, 40(4):329–336, 2009.

[9]Dianzi Liu, Vassili V Toroporov, Osvaldo M Querin, and David C Barton. Bilevel optimization of blended composite wing panels. *Journal of aircraft*, 48(1):107–118, 2011.

[10]Marco Montemurro, Angela Vincenti, and Paolo Vannucci. A two-level procedure for the global optimum design of composite modular structuresapplication to the design of an aircraft wing. *Journal of Optimization Theory and Applications*, 155(1):24–53, 2012.

[11]Anita Catapano and Marco Montemurro. A multi-scale approach for the optimum design of sandwich plates with honeycomb core. part ii: the optimisation strategy. *Composite Structures*, 118:677–690, 2014.

[12]Dianzi Liu, Vassili V Toropov, David C Barton, and Osvaldo M Querin. Weight and mechanical performance optimization of blended composite wing panels using lamination parameters. *Structural and Multidisciplinary Optimization*, 52(3):549–562, 2015.

[13]Rubens Zolar Gehlen Bohrer, Sérgio Frascino Müller de Almeida, and Mauricio Vicente Donadon. Optimization of composite plates subjected to buckling and small mass impact using lamination parameters. *Composite Structures*, 120:141–152, 2015.

[14]Thiago Assis Dutra and Sérgio Frascino Müller de Almeida. Composite plate stiffness multicriteria optimization using lamination parameters. *Composite Structures*, 133:166–177, 2015.

[15]Daniël Peeters and Mostafa Abdalla. Optimisation of variable stiffness composites with ply drops. In *56th AIAA/ASCE/AHS/ASC Structures, Structural Dynamics, and Materials Conference*, page 0450, 2015.

[16]Olivia Stodieck, Jonathan E Cooper, PM Weaver, and Paul Kealy. Optimization of tow-steered composite wing laminates for aeroelastic tailoring. *AIAA Journal*, 53(8):2203–2215, 2015.

[17]Graeme J Kennedy and JRRA Martins. A comparison of metallic and composite aircraft wings using aerostructural design optimization. In *14th AIAA/ISSMO multidisciplinary analysis and optimization conference, Indianapolis, IN*, 2012.

[18]Julien Marie Jan Ferdinand Van Campen. *Optimum lay-up design of variable stiffness composite structures*. TU Delft, Delft University of Technology, 2011.

[19]JMJF Van Campen and Zafer Gürdal. Retrieving variable stiffness laminates from lamination parameters distribution. In *Proceedings of the 50th AIAA/ASME/ASCE/AHS/ASC structures, structural dynamics and materials conference, Palm Springs, CA*, 2009.

[20]Grant Soremekun, Zafer Gürdal, Christos Kassapoglou, and Darryl Toni. Stacking sequence blending of multiple composite laminates using genetic algorithms. *Composite Structures*, 56(1):53–62, 2002.

[21]David B Adams, Layne T Watson, Zafer Gürdal, and Christine M Anderson-Cook. Genetic algorithm optimization and blending of composite laminates by locally reducing laminate thickness. *Advances in Engineering Software*, 35(1):35–43, 2004.

[22]John C Vassberg, Mark A DeHaan, S Melissa Rivers, and Richard A Wahls. Development of a common research model for applied CFD validation studies. *AIAA paper*, 6919:2008, 2008.

[23]Hong T Hahn and Stephen W Tsai. *Introduction to composite materials*. CRC Press, 1980.

[24]Zafer Gürdal, Raphael T Haftka, and Prabhat Hajela. *Design and optimization of laminated composite materials*. John Wiley & Sons, 1999.

[25]Zhangming Wu, Gangadharan Raju, and Paul M Weaver. Framework for the buckling optimization of variable-angle tow composite plates. *AIAA Journal*, 53(12):3788–3804, 2015.

[26]Terence Macquart, Marco T Bordogna, Paul Lancelot, and Roeland De Breuker. Derivation and application of blending constraints in lamination parameter space for composite optimisation. *Composite Structures*, 2015.

[27]Noud PM Werter and R. De Breuker. Aeroelastic tailoring and structural optimisation using an advanced dynamic aeroelastic framework. In *Proceedings of the International Forum on Aeroelasticity and Structural Dynamics, Saint Petersburg, Russia*, 2015.

[28]Etana A Ferede and Mostafa M Abdalla. Cross-sectional modelling of thin-walled composite beams. In *55th AIAA/ASMe/ASCE/AHS/SC Structures, Structural Dynamics, and Materials Conference*, page 0163, 2014.

[29]Krister Svanberg. A class of globally convergent optimization methods based on conservative convex separable approximations. *SIAM journal on optimization*, 12(2):555–573, 2002.

[30]Christos Kassapoglou. *Design and analysis of composite structures: with applications to aerospace structures*. John Wiley & Sons, 2013.

[31]Optibless - an open-source toolbox for the optimisation of blended stacking sequences (accepted). In *The seventeenth European Conference on Composite Materials (ECCM17)*, 2016.